

# Highly efficient resonant coupling of optical excitations in hybrid organic/inorganic semiconductor nanostructures

QIANG ZHANG<sup>1</sup>, TOLGA ATAY<sup>2</sup>, JONATHAN R. TISCHLER<sup>3</sup>, M. SCOTT BRADLEY<sup>3</sup>, VLADIMIR BULOVIĆ<sup>3</sup> AND A. V. NURMIKKO<sup>1,2\*</sup>

<sup>1</sup>Division of Engineering, Brown University, Providence, Rhode Island 02912, USA

<sup>2</sup>Department of Physics, Brown University, Providence, Rhode Island 02912, USA

<sup>3</sup>Department of Electrical Engineering and Computer Science, Massachusetts Institute of Technology, Cambridge, Massachusetts 02139, USA

\*e-mail: arto\_nurmikko@brown.edu

Published online: 19 August 2007; doi:10.1038/nnano.2007.253

The integration of organic and inorganic semiconductors on the nanoscale offers the possibility of developing new photonic devices that combine the best features of these two distinct classes of material. Such devices could, for example, benefit from the large oscillator strengths found in organic materials and the nonlinear optical properties of inorganic species. Here we describe a novel hybrid organic/inorganic nanocomposite in which alternating monolayers of J-aggregates of cyanine dye and crystalline semiconductor quantum dots are grown by a layer-by-layer self-assembly technique. We demonstrate near-field photon-mediated coupling of vastly dissimilar optical excitations in the two materials that can reach efficiencies of up to 98% at room temperature. By varying the size of the quantum dots and thus tuning their optical resonance for absorption and emission, we also show how the ability of J-aggregates to harvest light can be harnessed to increase the effective absorption cross section of the quantum dots by up to a factor of ten. Combining organic and inorganic semiconductors in this way could lead to novel nanoscale designs for light-emitting, photovoltaic and sensor applications<sup>1–4</sup>.

The concept of exploiting resonant energy transfer between organic and inorganic semiconductor materials to create nanoscale interfaces with useful electromagnetic properties was first suggested by Agranovich and co-workers in 1999 (ref. 5), and has recently been demonstrated<sup>6–8</sup>. The coupling takes place between excitons—bound electron–hole pairs—within the hybrid composite. The most common form of exciton in an organic semiconductor is a Frenkel exciton, which is tightly localized on a single molecular site and moves as a unit through the molecules. On the other hand, the Wannier–Mott excitons found in inorganic semiconductors can span across hundreds of lattice unit cells. To fully exploit the electromagnetic coupling between these different types of excitons, one must seek for materials that exhibit strong photon–matter interactions. As the key ingredients for the novel nanocomposite material system reported in this paper, colloidal semiconductor quantum dots

(QDs) offer superior photostability and wavelength tunability<sup>9</sup>, and J-aggregates (self-assembled molecules in a regular linear arrangement in which the transition moments of individual monomers are aligned parallel to the line joining their centres) have exceptional optical oscillator strength<sup>10</sup>. Unlike prior demonstrations of the energy transfer in heterostructures involving semiconductor quantum wells<sup>6,11</sup>, the optical attributes of our QD/J-aggregate hybrids are highlighted by their robust excitonic transitions at room temperature with spectrally concentrated absorption and emission strengths.

The layer-by-layer (LBL) assembly approach<sup>12</sup> is a general preparative technique for creating multilayer thin films whose thickness can be controlled precisely on the nanometre scale. It has been successfully applied to the fabrication of functional thin films of material species ranging from dyes<sup>13</sup> to nanoparticles<sup>14</sup>, proteins and DNA strands<sup>15</sup>, and so on. Recently, exceptionally large absorption coefficients ( $\geq 10^6 \text{ cm}^{-1}$ ) at room temperature have been measured in ultrathin J-aggregate films prepared by this technique<sup>16</sup>. Figure 1a schematically shows the typical structure of the hybrid organic/inorganic (J-aggregate/QD) LBL films that we synthesized for the present study, along with the chemical structures of the constituents. In the hybrid film, a single monolayer J-aggregate of cyanine dye (TDBC) was sandwiched between two monolayers of CdSe–ZnS core–shell structured QDs, with polyelectrolyte (PDDA) acting as the ultrathin ‘molecular glue’. We focus in this paper on two types of hybrid films, one with QD emission centred at 548 nm (referred to as film I) and the other at 653 nm (referred to as film II), thus providing contrasting cases of excitation coupling with respect to the fixed J-aggregate emission at 594 nm. Representative atomic force microscopy (AFM) images of hybrid film II and two additional QD and J-aggregate reference films are shown in Fig. 1b–d. Height analysis on the images revealed that the TDBC/PDDA bilayer film thickness was approximately 3.3 nm, in good correspondence with the monolayer thicknesses of TDBC J-aggregate ( $\sim 1.8$ –2 nm) and PDDA (1.3 nm) previously

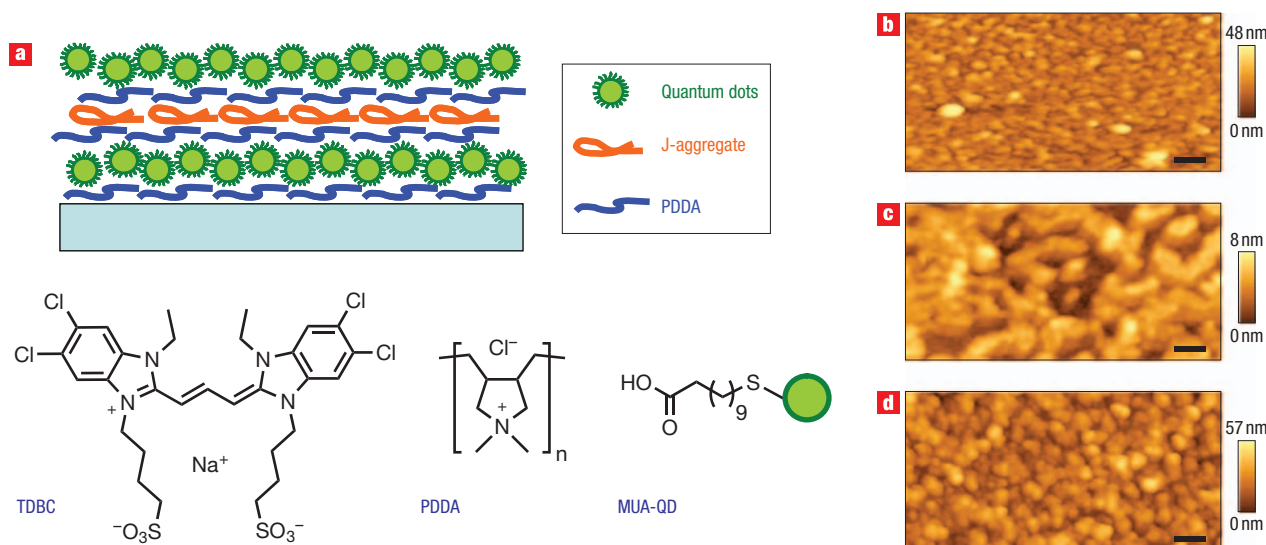


**Figure 1** Hybrid organic–inorganic (J-aggregate/QD) multilayer film deposited by LBL assembly. **a**, Schematic of the hybrid film layer structure: a monolayer J-aggregate of 5,6-dichloro-2-[3-[5,6-dichloro-1-ethyl-3-(3-sulphopropyl)-2(3H)-benzimidazolide]-1-propenyl]-1-ethyl-3-(3-sulphopropyl) benzimidazolium hydroxide (TDBC) is sandwiched between two monolayers of CdSe–ZnS QDs, joined by monolayers of poly(diallyldimethylammonium chloride) (PDDA). Molecular structures of TDBC, PDDA and MUA are illustrated in the lower panel. **b–d**, AFM images of the LBL-grown films, consisting of a monolayer of QDs ( $\lambda_{\text{em}} = 653 \text{ nm}$ ) (PDDA/QD) (**b**), a monolayer of J-aggregate (PDDA/TDBC/PDDA) (**c**), and the hybrid film II (**d**). The scale bars in **b–d** are 100 nm.

acquired by neutron scattering<sup>17</sup> and X-ray reflectivity<sup>18</sup> measurements. The average diameters of the 11-mercaptopundecanoic acid (MUA)-capped QDs in film I and film II were determined to be 5 nm and 9 nm, respectively.

In hybrid film I, we studied the excitonic energy transfer from the QDs to the J-aggregates, whose spectral relationship is illustrated in Fig. 2a. The greenish QD emission is spectrally distinct from that of the J-aggregate, yet provides sufficient spectral overlap with the J-band absorption for electromagnetic interaction. In the absorbance spectrum of film I shown in the inset of Fig. 2b, we note that the QD absorption became dominant over that of the J-aggregate for wavelengths below 450 nm. We next chose to set the photoexcitation at  $\lambda_{\text{ex}} = 380 \text{ nm}$  to ensure a dominant input excitation to the QDs alone. Shown in Fig. 2b, the resulting photoluminescence (PL) spectrum of film I exhibited a pronounced quenching effect of the QD emission by nearly 98%, with a simultaneous boost of the J-aggregate luminescence. Such luminescence contrast is consistent with the quantum yields of the QDs (50%) and J-aggregate (15%) obtained through separate PL and absorption measurements.

Next, time-resolved PL studies of the hybrid film I were carried out using both streak camera and time-correlated single photon counting (TCSPC) techniques. The detection wavelength was chosen to assure easy spectral isolation of the QD emission as detailed in Fig. 2d. In Fig. 2c, we show how the QD PL decay in hybrid film I was significantly accelerated with respect to that of the QD control, but displayed a non-exponential nature that may be a consequence of film inhomogeneity. In examining the details of the excitation transfer dynamics in Fig. 2e, a pronounced elongation of the J-aggregate PL decay in film I was detected in comparison to the J-aggregate control, indicating the continuity of energy transfer following the photoexcitation. The discrepancy between the temporal behaviours of QDs and J-aggregates in the hybrid film was attributed to the presence of multiple energy transfer rates and small-residue J-aggregate absorption at the excitation wavelength. The overall behaviours can be well

described by a simple rate equation model, which yielded a fast energy transfer rate of  $0.05 \text{ ps}^{-1}$  accounting for 76% of the total QD population.

In a role reversal, efficient energy transfer from J-aggregates to QDs could lead to a hybrid material that brings together the benefits from both constituents, namely large absorption strength and high quantum efficiency. We explored this in hybrid film II, where the QD emission was offset to the lower energy side of the J-aggregate emission, as displayed in Fig. 3a. The absorbance spectrum of film II is shown in the inset of Fig. 3b. Demonstrating excitonic excitation transfer, Fig. 3b presents the PL spectrum of film II upon illumination at the J-band absorption peak ( $\lambda_{\text{ex}} = 589 \text{ nm}$ ). After spectral decomposition and analysis, we measured that the QD emission in film II was enhanced tenfold in relation to the QD control film, but its spectral profile and position were preserved.

Photoluminescence excitation (PLE) measurement of the hybrid film II probing at the QD emission peak ( $\lambda_{\text{em}} = 653 \text{ nm}$ ) offered another useful perspective for this interesting phenomenon. As depicted in Fig. 3d, a pronounced feature closely resembling the J-band absorption appeared atop the QD PLE background. Quantitative analysis of the PLE spectrum has enabled us to extract the energy transfer efficiency from J-aggregates to QDs as follows. We express the PLE spectrum of film II with residual J-aggregate emission at 653 nm subtracted as  $[\text{Abs}^{\text{J}}(\lambda) \times \eta(\lambda) + \text{Abs}^{\text{QD}}(\lambda)] \times \text{QY} \times F(\lambda)$ . Here,  $\text{Abs}^{\text{J}}(\lambda)$  and  $\text{Abs}^{\text{QD}}(\lambda)$  are the absorption of J-aggregates and QDs, respectively;  $\eta(\lambda)$  is the energy transfer efficiency; QY is the quantum yield of the QD;  $F(\lambda)$  describes all other factors that are sample-independent, such as instrumentation response. Accounting for factors QY and  $F(\lambda)$  by a proper reference sample, the effective QD absorption, namely  $\text{Abs}^{\text{J}}(\lambda) \times \eta(\lambda) + \text{Abs}^{\text{QD}}(\lambda)$ , can be obtained from the PLE spectrum. The result is summarized in Fig. 3c, in conjunction with the absorption spectra of film II and the QD control. Then  $\eta(\lambda)$  can be derived from the ratio of the differences between these curves, as plotted

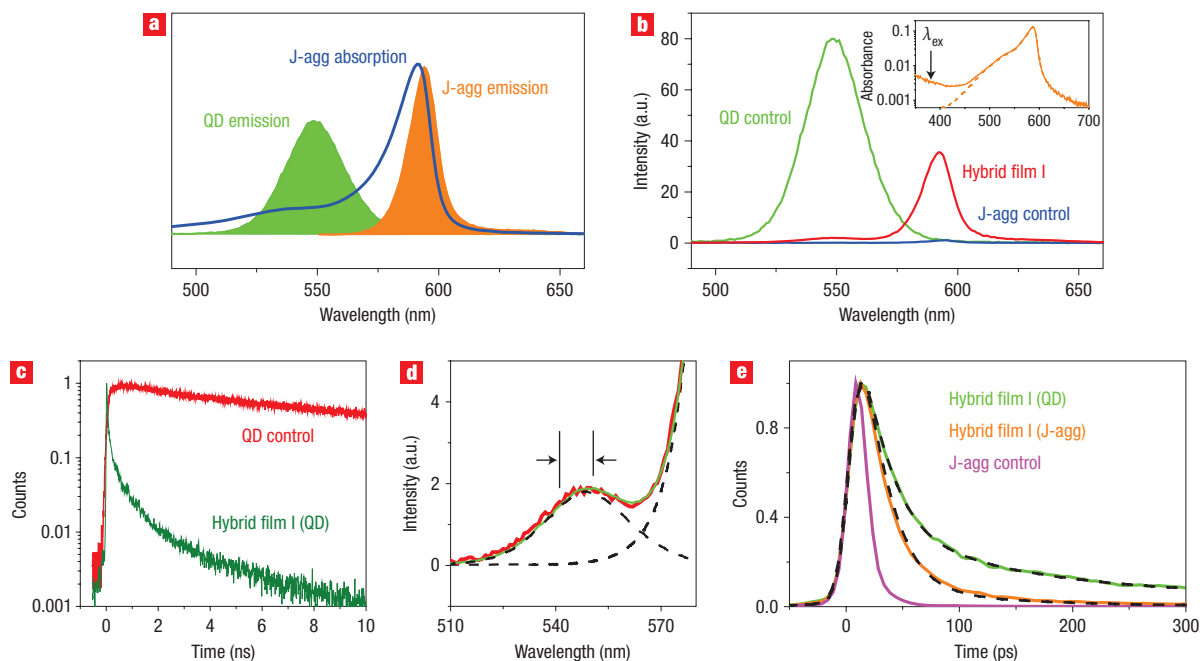


**Figure 2** Optical characterizations of hybrid film I to explore resonance energy transfer from QDs to J-aggregates. **a**, Absorption (blue) and emission (orange) spectra of the TDBC J-aggregate film, as well as the emission spectrum of the QDs ( $\lambda_{em} = 548$  nm) (green). **b**, PL spectra of the hybrid film I (red), QD control film (green) and the J-aggregate control film (blue). The excitation wavelength was set to be 380 nm. The inset shows the absorbance spectrum of the hybrid film I (solid line) in semi-logarithmic scale. The QD contribution is visible in the wavelength range below 450 nm, with respect to the roll-off of the J-aggregate absorption (dashed line) towards shorter wavelengths. **c**, Time-resolved QD PL decay traces (normalized) from the QD control film (red) and the hybrid film I (green), detected in the neighbourhood of 546 nm. **d**, PL spectrum of the hybrid film I (red) was fitted by a linear combination (green) of the QD and the J-aggregate emissions (dashed line). The optical detection bandwidth was 10 nm (indicated by the arrows) and 3 nm, for streak camera and TCSPC, respectively. It is estimated that more than 97% of the photons collected within the detection band from hybrid film I were contributed by the QD emission. **e**, Time-resolved PL decay traces measured by streak camera at picosecond timescale, from the QD in hybrid film I (green), the J-aggregate in hybrid film I (orange) and the J-aggregate control film (purple). The J-aggregate emission was detected with 10-nm bandwidth centred at 600 nm. The fitting curves (dashed lines) for the former two traces were generated in a rate equation model and were convolved with the instrumentation response function of the streak camera. The model assumed the presence of three different energy transfer time constants, fitted to be 20 ps, 110 ps and 1,100 ps, respectively.

in Fig. 3e. We observed an order of magnitude increase in the effective absorption of QD at the J-aggregate absorption peak, where  $\eta$  was determined to be about 22%. Thus we demonstrate the potency of using an organic aggregate as the light-harvesting antenna to significantly enlarge the absorption cross-section of an inorganic semiconductor.

In examining the microscopics behind such pronounced experimental effects, we first note that the contribution of radiative energy transfer (through propagating photon emission and subsequent absorption) should be practically negligible, because the single-pass absorption through a monolayer of QD in film II is only a fraction of a percent at the wavelength range of interest. Among non-radiative energy transfer possibilities, Dexter transfer through electron exchange<sup>19</sup> is also unlikely. Our experiments show no evidence of interlayer electronic crosstalk in either J-aggregate or QD multilayer LBL films, which would have been reflected in changes in exciton confinement energy and radiative lifetime<sup>20</sup>. Hence, regarding our results in both hybrid films I and II, we argue that near-field dipole–dipole coupling between QD and J-aggregate subcomponents is the primary mechanism for rapid excitonic energy transfer. The effect is analogous to the Förster transfer process<sup>21</sup> in purely molecular systems, but it is occurring here between two highly dissimilar electronic materials in a quasi-two-dimensional setting.

We next calculate the excitation transfer rate and efficiency in a classical model, describing a single-dipole type or J-aggregate type of donor in the proximity of a thin acceptor layer<sup>22</sup>. Such a model has been shown to be equivalent to the Förster formalism when molecular donors and acceptors are considered. In the case of hybrid film I (QD emitter and J-aggregate acceptor layer), we assume the acceptor layer to be interacting only with the polarization electric-field component oscillating in the plane of the layer. This corresponds to the usual experimental situation for one- and two-dimensional J-aggregates<sup>23,24</sup>. The energy transfer rate can thus be written as  $\Gamma \approx \tau_{QD}^{-1}(d_0/d)^4$  in the proximity field approximation. Here,  $\Gamma$  is the averaged energy transfer rate from QDs to J-aggregates when the QD transition dipole moment orientation is random;  $\tau_{QD}$  is the PL decay time constant of the QD in the absence of J-aggregate;  $d$  is the separation between the centres of the QD and J-aggregate layers;  $d_0$  is the energy transfer characteristic length, defined by  $(d_0)^4 \equiv (4\pi)^{-4}(3/2)^3 n^{-4} q^{QD} \int \lambda^4 A^I(\lambda) f^{QD}(\lambda) d\lambda$  (ref. 22), in which  $n$  is the index of refraction of the media (assumed to be PDDA),  $A^I(\lambda)$  is the absorption spectrum of the J-aggregate acceptor layer upon normal incidence,  $q^{QD}$  is the quantum yield of QD and  $f^{QD}(\lambda)$  is the normalized emission spectrum of QD. As our measurements yielded values for  $n = 1.53$  and  $q^{QD} = 50\%$ , it follows that  $d_0 = 17.2$  nm. Thus, by taking  $d = 4.8$  nm

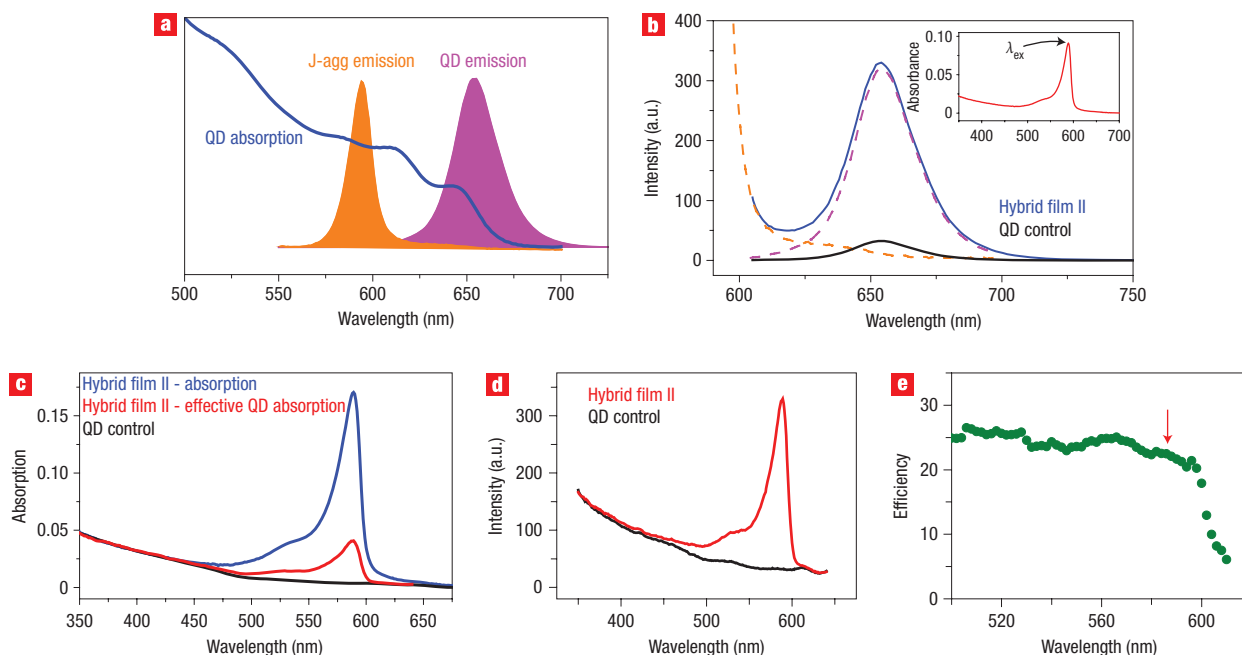


**Figure 3** Optical characterizations of hybrid film II to explore resonance energy transfer from J-aggregate to QD. **a**, The emission spectrum of TDBC J-aggregate ( $\lambda_{em} = 594$  nm) (orange) spectrally overlaps with the QD absorption (blue), but the QD emission (purple) is centred at 653 nm. **b**, PL spectra of the hybrid film II (blue) and the QD control film (black). The excitation wavelengths were set to be at  $\lambda_{ex} = 589$  nm, the peak of J-band absorption. Contributions of the QD emission (purple dashed line) and the J-aggregate emission (orange dashed line) to the PL of hybrid film II are separated. The absorbance spectrum of hybrid film II is shown in the inset. **c**, The effective QD absorption spectrum (red), expressed as  $Abs^e(\lambda) \times \eta(\lambda) + Abs^{QD}(\lambda)$ , was derived from the PLE spectrum shown in **d**. The absorption spectra of hybrid film II (blue) and the QD control film (black) were obtained by measuring both the transmission and reflection spectra of each film. **d**, The raw PLE spectrum of hybrid film II (red) and QD control (black) when detecting at the QD emission peak. **e**, J-aggregate to QD energy transfer efficiency  $\eta(\lambda)$  calculated using the data shown in **c**. The arrow indicates the peak of J-band absorption.

and  $\tau_{QD} = 6.9$  ns from the AFM and TCSPC measurements,  $\Gamma$  is estimated to be  $0.024$  ps $^{-1}$ . Such a calculated result compares reasonably well with the measured fast energy transfer rate in film I given the uncertainty in determining actual  $d$ . As for hybrid film II (J-aggregate emitter and QD acceptor layer), simple analytical expression of energy transfer efficiency  $\eta$  is not available. However, if we restrict our discussion to a linear J-aggregate model where the exciton delocalization length  $l$  satisfies  $l \ll \lambda$ , and assume isotropic acceptor layers, we then found  $\eta$  can be well described by an empirical formula as  $\eta = [1 + (1 - \alpha)(d/d_0)^2 + \alpha(d/d_0)^4]^{-1}$ . Here, parameters  $\alpha$  and  $d_0$  are determined numerically given the absorption of the QD layer  $A^{QD}$ , the quantum yield of J-aggregate  $q^J$ , as well as  $n$  and  $l$ . In particular,  $\alpha \approx 0$  when  $l \gg d_0$  and  $\alpha \approx 1$  when  $l \ll d_0$ . Our separate ultrafast frequency-resolved pump-probe spectroscopy experiments<sup>25</sup> on LBL-grown TDBC J-aggregate films show that  $l$  typically measures as much as 16 monomer units (see Supplementary Information, Fig. S1). Given  $A^{QD} = 0.19\%$ ,  $q^J = 22\%$  from direct measurements, and assuming TDBC aggregate unit cell length to be 1.3 nm (ref. 17), we find  $\alpha = 0.1$  and  $d_0 = 4.4$  nm (the presence of two acceptor layers has been taken into account). With  $d = 6.8$  nm from AFM measurement, the overall energy transfer efficiency should thus be  $\eta = 27\%$ , which is in reasonable agreement with the experimentally measured value. The model points out that substantial improvement of  $\eta$  should be achievable by optimizing both the quantum yield of J-aggregate and the donor–acceptor spectral overlap. Indeed, we recently demonstrated  $\eta = 38\%$  from J-aggregate to QD through the implementation of a different

type of J-aggregate with blueshifted emission at 470 nm (see Supplementary Information, Figs S2, S3).

In summary, we have described the synthesis and performance of a hybrid organic–inorganic nanoscale optical material that combines semiconductor QDs and cyanine dye J-aggregates. Highly efficient energy transfer has been demonstrated between the two subcomponents. Moreover, the direction of the energy flow can be controlled by tuning the spectral properties of the QDs. The ability to activate intense near-field electromagnetic interactions between two very different semiconductor species presents an exciting opportunity for the construction and optimization of new types of functional nanocomposites for photonic applications. It also suggests the possibility of reaching the strong coupling regime where the hybridization of Frenkel and Wannier–Mott excitons has been proposed to lead to attractive linear and nonlinear optical properties<sup>26</sup>.

## METHODS

### PREPARATION OF WATER-SOLUBLE ANIONIC QUANTUM DOTS

CdSe–ZnS core–shell structured QDs in decane (Molecular Probes) were water-solubilized by surface ligand exchange with MUA. The process was carried out in chloroform, which typically contains 0.5  $\mu$ M QDs, 28 mM MUA and 41 mM tetramethylammonium hydroxide (TMAH). Phase segregation occurred when adding deionized water into the solution. MUA-capped QDs were transferred into the water phase, forming a uniform dispersion. The aqueous QD dispersion was extracted out. Excessive ligands were removed by purifying the particle solution through centrifugal filters followed by dilution in deionized water at least three times.

## LBL ASSEMBLY

The hybrid film was deposited in a dip-coating fashion by immersing a thoroughly cleaned quartz plate into the aqueous solutions of each species sequentially, in an order according to the film structure shown in Fig. 1a. The concentrations and pH values of the solutions are as follows: QD, 50 nM, pH 8.0; TDBC, 50  $\mu$ M, pH 8.0; PDDA (molecular weight 400–500 K) 0.58 mM, NaCl 0.5 M, pH 7.0. The TDBC and PDDA solutions were sonicated for 30 min before use. The immersion times were set to be 150 min, 15 min and 15 min for the QD, TDBC and PDDA solutions, respectively, followed by a 1 min rinse in deionized water. Care was taken throughout the deposition to shield the dye solution and films from light. After deposition, the film on one side of the plate was removed with methanol. The QD and J-aggregate control films were fabricated following a similar procedure. Tapping-mode AFM (Explorer, Veeco) was used for surface characterization of the LBL films. For QD-diameter measurement, test films with low QD surface density were used.

## OPTICAL AND SPECTROSCOPIC MEASUREMENTS

The transmission and reflection spectra of the films (near normal incidence) were determined using a spectrophotometer (Cary 500i UV-Vis-NIR, Varian) with a spectral bandwidth of 2 nm. The photoluminescence and photoluminescence excitation spectra were collected with a fluorescence spectrophotometer (Cary Eclipse, Varian). The spectral bandwidth was set to be 5 nm for both excitation and detection beams, which were tilted at 45° to the film normal. The quantum yield (QY) of the MUA-capped QDs in aqueous dispersion was obtained through absorption and PL measurements by comparing with those in decane, for which the QY is known. The QY of the J-aggregate film was derived using the QD control film as reference. The refractive index of PDDA (spin-cast film) was measured with an ellipsometer (AutoEL, Rudolph Research).

A custom-made time-correlated single photon counting (TCSPC) setup and a synchroscan streak camera (C1587, Hamamatsu) was used for time-resolved photoluminescence measurement. A frequency-doubled ultrafast Ti:Sapphire laser (MIRA 900, Coherent) operating at 380 nm acted as the excitation source. The laser pulse width was measured to be 120 fs. In TCSPC measurement, the laser repetition rate was down-converted to 1.9 MHz by an acoustic optical modulator. The optical detection system was composed of a monochromator (SpectraPro, Acton Research) and a photon-counting microchannel plate photomultiplier tube (R3809U-50, Hamamatsu). In the streak camera measurement, the detected PL was filtered through 10-nm-wide bandpass filters at 546 nm (Chroma) or 600 nm (CVI). The streak image was projected onto a cryogenic cooled charge-coupled device (Princeton Instruments).

Received 30 May 2007; accepted 13 July 2007; published 19 August 2007.

## References

1. Coe, S., Woo, W.-K., Bawendi, M. & Bulović, V. Electroluminescence from single monolayers of nanocrystals in molecular organic devices. *Nature* **420**, 800–803 (2002).
2. Huynh, W. U., Dittmer, J. J. & Alivisatos, A. P. Hybrid nanorod–polymer solar cells. *Science* **295**, 2425–2427 (2002).
3. Medintz, I. L. *et al.* Self-assembled nanoscale biosensors based on quantum dot FRET donors. *Nature Mater.* **2**, 630–638 (2003).
4. Becker, K. *et al.* Electrical control of Förster energy transfer. *Nature Mater.* **5**, 777–781 (2006).
5. Basko, D., La Rocca, G. C., Bassani, F. & Agranovich, V. M. Förster energy transfer from a semiconductor quantum well to an organic material overlayer. *Eur. Phys. J. B* **8**, 353–362 (1999).
6. Blumstengel, S., Sadofev, S., Xu, C., Puls, J. & Henneberger, F. Converting Wannier into Frenkel excitons in an inorganic/organic hybrid semiconductor nanostructure. *Phys. Rev. Lett.* **97**, 237401 (2006).
7. Anikeeva, P. O. *et al.* Photoluminescence of CdSe/ZnS core/shell quantum dots enhanced by energy transfer from a phosphorescent donor. *Chem. Phys. Lett.* **424**, 120–125 (2006).
8. Heliotis, G. *et al.* Hybrid inorganic/organic semiconductor heterostructures with efficient non-radiative energy transfer. *Adv. Mater.* **18**, 334–338 (2006).
9. Alivisatos, A. P. Semiconductor clusters, nanocrystals and quantum dots. *Science* **271**, 933–937 (1996).
10. Burn, P. W. Aspects of structure and energy transportation in artificial molecular assemblies. *Annu. Rev. Phys. Chem.* **44**, 37–60 (1993).
11. Acherermann, M. *et al.* Energy-transfer pumping of semiconductor nanocrystals using an epitaxial quantum well. *Nature* **429**, 642–646 (2004).
12. Kotov, N. A. Ordered layered assemblies of nanoparticles. *Mater. Res. Bull.* **36**, 992–997 (2001).
13. Ariga, K., Lvov, Y. & Kunitake, T. Assembling alternate dye–polyion molecular films by electrostatic layer-by-layer adsorption. *J. Am. Chem. Soc.* **119**, 2224–2231 (1997).
14. Aliev, F. G. *et al.* Layer-by-layer assembly of core–shell magnetite nanoparticles: effect of silica coating on interparticle interactions and magnetic properties. *Adv. Mater.* **11**, 1006–1010 (1999).
15. Decher, G., Lehr, B., Lowack, K., Lvov, Y. & Schmitt, J. New nanocomposite films for biosensors: layer-by-layer adsorbed films of polyelectrolytes, proteins or DNA. *Biosens. Bioelectron.* **9**, 677–684 (1994).
16. Bradley, M. S., Tischler, J. R. & Bulović, V. Layer-by-layer J-aggregate thin films with a peak absorption constant of  $10^6$  cm<sup>-1</sup>. *Adv. Mater.* **17**, 1881–1886 (2005).
17. von Berlepsch, H. *et al.* Supramolecular structures of J-aggregates of carbocyanine dyes in solution. *J. Phys. Chem. B* **104**, 5255–5262 (2000).
18. Mashl, R. J., Grönbeck-Jensen, N., Fitzsimmons, M. R., Lütt, M. & Li, D. Theoretical and experimental adsorption studies of polyelectrolytes on an oppositely charged surface. *J. Chem. Phys.* **110**, 2219–2225 (1999).
19. Turro, N. J. *Modern Molecular Photochemistry* (University Science Books, Mill Valley, California, 1991).
20. So, F. F. & Forrest, S. R. Evidence for exciton confinement in crystalline organic multiple quantum-wells. *Phys. Rev. Lett.* **66**, 2649–2652 (1991).
21. Scholes, G. D. Long-range resonance energy transfer in molecular systems. *Annu. Rev. Phys. Chem.* **54**, 57–87 (2003).
22. Kuhn, H. Classical aspects of energy transfer in molecular systems. *J. Chem. Phys.* **53**, 101–108 (1970).
23. Hirano, Y., Ohkubo, M. A., Tokuoka, Y., Kawashima, N. & Ozaki, Y. Orientation of merocyanine dye in mixed Langmuir–Blodgett films investigated by visible absorption spectroscopy. *Mol. Cryst. Liq. Cryst.* **445**, 93–99 (2006).
24. Inoue, T., Moriguchi, M. & Ogawa, T. Molecular orientation of oxocyanine dye in an LB film determined by second harmonic generation and polarized absorption techniques. *Thin Solid Films* **350**, 238–244 (1999).
25. van Burgel, M., Wiersma, D. A. & Duppen, K. The dynamics of one-dimensional excitons in liquids. *J. Chem. Phys.* **102**, 20–33 (1995).
26. Agranovich, V. M., Basko, D. M., La Rocca, G. C. & Bassani, F. Excitons and optical nonlinearities in hybrid organic–inorganic nanostructures. *J. Phys. Condens. Matter* **10**, 9369–9400 (1998).

## Acknowledgements

This work was supported by the US Department of Energy and the National Science Foundation. We would like to thank S. Sun for support in sample preparation, G. T. R. Palmore for making the fluorescence spectrophotometer available for our use and R. Zia for valuable discussions. Correspondence and requests for materials should be addressed to A.V.N. Supplementary information accompanies this paper on [www.nature.com/naturenanotechnology](http://www.nature.com/naturenanotechnology).

## Competing financial interests

The authors declare no competing financial interests.

Reprints and permission information is available online at <http://npg.nature.com/reprintsandpermissions/>